Journal of South American Earth Sciences 48 (2013) 106–122

Contents lists available at ScienceDirect

Journal of South American Earth Sciences

journal homepage: www.elsevier.com/locate/jsames

Crustal velocity structure beneath the western Andes of Colombian using receiver-function inversion

Hugo Monsalve [a,*], Javier F. Pacheco [c], Carlos A. Vargas [b], Yorly A. Morales [a]

[a] Universidad del Quindío, Colombia, CEIFI, Grupo Quimbaya, Armenia, Colombia
[b] Universidad Nacional de Colombia, Sede Bogotá, Grupo de Geofísica, Colombia
[c] OVSICORI-UNA, Universidad Nacional de Costa Rica, Colombia

ARTICLE INFO

Article history:
Received 10 August 2012
Accepted 1 September 2013

Keywords:
Receiver function
Moho
Teleseismic earthquakes
Colombia
Western Cordillera
Central Cordillera

ABSTRACT

Analysis of teleseismic records obtained in two broadband seismic stations of three components located on the Andean region of Colombia is presented in this work. The two stations are located at the Western Cordillera (WC), station BOL, and at the Central Cordillera (CC), station PBLA. The analysis of seismograms was performed by inversion of the receiver functions (RF) in order to obtain the crustal velocity structure beneath the receivers. The receiver function is a spectral ratio obtained from teleseismic earthquakes recorded by broadband seismic stations, which allows the calculation of the velocity structure beneath the receiver by removing source effects in the horizontal components of the seismic traces. Data stacking was performed in order to improve signal to noise ratio and then the data was inverted by using two optimization algorithms: a genetic algorithm (GA), and a simulated annealing algorithm (SA). The present work calculates the receiver functions using teleseismic earthquakes at epicentral distances (Δ) ranging between 30° and 90° and recorded at the two stations within the years 2007 and 2009.

Delay times between P and PS waves converted at the Moho boundary were used to constrain the velocity structure. The receiver functions at the stations were generated from seismic events within a broad range of back azimuth. Data from gravity and magnetism were also used during the geophysical survey. The depth of the Moho boundary was found to be at 40 km in the WC beneath station BOL and at 43 km in the CC beneath station PBLA. The upper crust, with a thickness of 5 km, is characterized by a shear wave velocity of about 3.0 km s^{-1}; the shallower layers, at approximately 1.0 km, have shear wave velocities between 2.2 and 2.6 km s^{-1}, which corresponds to sediments overlying the upper crust. These observations support the hypothesis of a thickness of the crust at the root of the mountain range to be between 32 and 50 km. The calculated receiver functions were compared with artificial ones generated from the inversion of 48000 models of horizontal layers for each station using a GA and an SA that allowed a satisfactory coverage of all the sample space in order to avoid non-unique solutions. Beneath station BOL a moderate low-velocity zone (LVZ) was found, which was caused by accretionary processes of the ophiolite complex in the WC.

1. Introducción

In order to know the crustal velocity structure several methodologies have been proposed; one of them is the receiver function methodology. Through this technique, it is possible to retrieve information to constrain subsurface regional geology.

The receiver function is an approximation of the crust-mantle transfer function for an incident teleseismic P wave (Burdick and Langston, 1977; Langston, 1977, 1979; Zhang and Langston, 1995). Nowadays, many research activities incorporate receiver function studies to analyze and model crustal structure, the uppermost mantle, or the subducting plates (e.g., Langston, 1977; Owens, 1987; Lapp et al., 1990; Gurrola et al., 1995; Baker et al., 1990; Shibutani et al., 1996; Ozalaybey et al., 1997; Bump and Sheenan, 1998).

The calculation of receiver functions in a three-component seismic station is a technique, pioneered by Langston (1979) and later modified and improved by Ammon (1991), used to obtain the effect that the subsurface structure has on a seismic station by removing the source effects on the horizontal components of the seismic traces.

Due to the tectonics and geodynamics setting in the study area, there is a very complex lithologic heterogeneity with topographic variations from 0 m to 5800 m above mean sea level (AMSL), an active continental deformation with the generation of great mountain ranges, and the presence of valleys and extensive coastal

* Corresponding author.
E-mail address: hugom@uniquindio.edu.co (H. Monsalve).

0895-9811/$ – see front matter © 2013 Elsevier Ltd. All rights reserved.
http://dx.doi.org/10.1016/j.jsames.2013.09.001

zones (see Fig. 1); this implies that the values of the crustal thickness varies from one place to another. It is possible to find the highest values in the mountainous regions of the Andes and the lowest values in the coastal regions.

Florez and Osorio (2010) suggested that the crust in the Western Cordillera (WC) and the Central Cordillera (CC) is divided into two sections: the upper crust, characterized by P-wave velocities smaller than 6.0 km s^{-1}; and the lower crust, characterized by P-wave velocities between 5.0 and 7.4 km s^{-1} along with lower velocity gradients. Same authors obtained a ratio Vp/Vs = 1.77 which was estimated by a one-dimensional model.

In this study the crustal structure obtained by the receiver functions was separated through modeling the upper and lower crust in the two mountain ranges based on velocity gradient variations, which are observed in the velocity structure profiles. We have used the receiver function analysis of Ammon et al. (1990) along with genetic algorithms and simulated annealing to obtain a one-dimensional S-wave velocity model beneath two stations, BOL and PBLA. Genetic algorithms and simulated annealing allow trying a great number of optimal alternatives that may fit the observed data; thus reducing the uncertainty over the solution. Station acronyms (BOL and PBLA) will be used hereafter to refer to the seismological stations which are located at the WC, in the municipality of Bolivar, and at the CC, in the municipality of La Virginia-Peñas Blancas respectively. Finally, the results will be compared with the gravity and magnetic surveying performed by Alexander et al. (2010).

2. Geology

Defining composition and structure of the Andean range in central-western Colombia gives important information regarding its orogenic cycle and its crustal structure, as well as construct a reliable regional seismotectonic model.

The CC (Figs. 1 and 2) is mainly composed of plutonic and metamorphic rocks coated by isolated remnants of marine sedimentary rocks from the Cretaceous. There is a Precambrian core of granulite facies in metamorphic rocks which are the product of a continent–continent type collision during the late Precambrian (Kroonemberg, 1982; Restrepo-Pace, 1995), sandstones as well as green rocks, cataclastic schists, serpentine rocks, granodiorites and

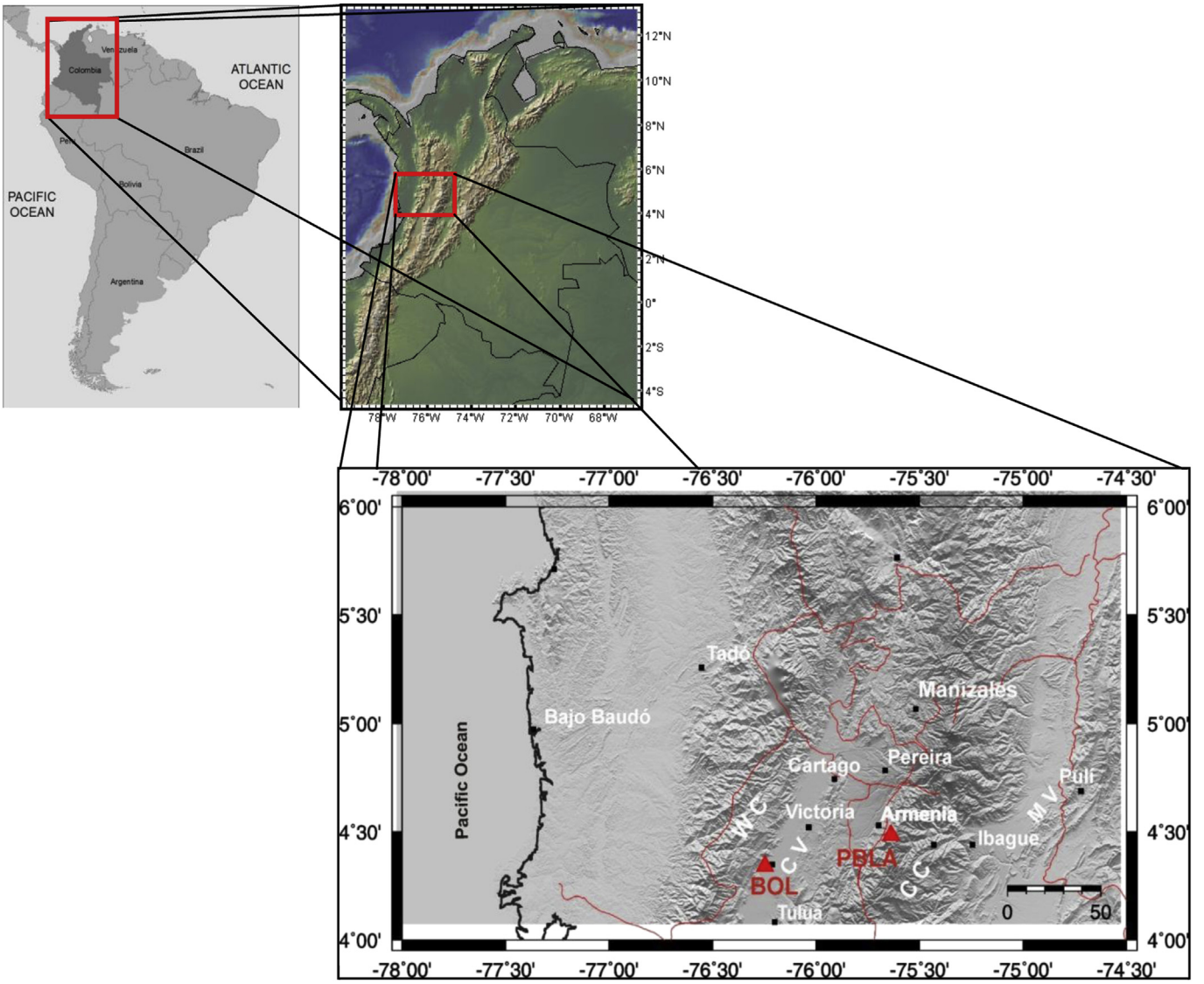

Fig. 1. Study area: The red triangles show the location of the two broadband seismic stations BOL and PBLA. The small black squares show cities nearby the study zone. (WC) Western Cordillera, (CC) Central Cordillera, (CV) Cauca Valley, (MV) Magdalena Valley. (For interpretation of the references to color in this figure legend, the reader is referred to the web version of this article.)

diorites from the Cretaceous. The lithologic varieties and folded foliation of these rocks with dip North-North-East were mapped by Grosse (1926), Botero (1963) y Feininger et al. (1972). One of the largest volcanic systems from the late Cenozoic in the Northern Andes is the Ruiz-Tolima volcanic complex, which is covering the older units in the zone. Fig. 2 shows these geologic units.

On the other hand, the WC is one of the largest ophiolite complexes of the world, which extends along Costa Rica, Panamá, Colombia and Ecuador (Kellogg and Vega, 1995). This mountain range is composed by marine layers from the Cretaceous, metamorphic rocks, toleitic basalts, mafic andesites, and quartz diorites from the Tertiary. The most common rock types are sandstones, greywackes, lutites and mafic rocks (green rocks). The most recent uplift of the three mountain ranges (Western, Central, and Eastern Cordillera) took place during the late Cenozoic; the uplifts are limited by faults and steep folds with North azimuth. Fig. 2 shows the geologic units where PBLA and BOL stations were emplaced.

3. Data

3.1. Selection of the seismic stations and the seismic traces

Two sites were chosen in order to locate the two stations and inferring the velocity structure underneath; one site on the CC and another site on the WC. The stations had to be placed on outcropping rock. The first station (PBLA) was placed at Peñas Blancas in the CC and the second station (BOL) was placed nearby Bolivar, Valle del Cauca, in the WC. By the time of the project, these were the two only operational broadband seismic stations in the country and the chosen places had to meet two more criteria, security and proximity to the Seismological Observatory of the Universidad del Quindio in Armenia city. By the end of 2012, ten more broadband stations were installed; and by 2014 other ten stations are expected to be operating in the network.

For the calculation of the receiver functions, teleseismic earthquakes recorded by the broadband stations were used. Stations BOL and PBLA (Table 1) are mobile stations and have seismograms from earthquakes recorded since November 2007.

81 teleseismic earthquakes were recorded at station BOL, and 44 teleseismic earthquakes were recorded at station PBLA (Jaramillo, 2010). Seismograms with a low signal-to-noise ratio (SNR) and those with evident source effects were omitted. Also, the seismograms for which the receiver function looked awkward were dismissed. This selection process left 8 optimal seismic traces in BOL and 10 optimal seismic traces in PBLA in order to obtain groups in the best possible azimuthal position.

3.2. Record processing

Once the files of the teleseismic earthquakes recorded at stations BOL and PBLA were obtained, the basic processing procedures

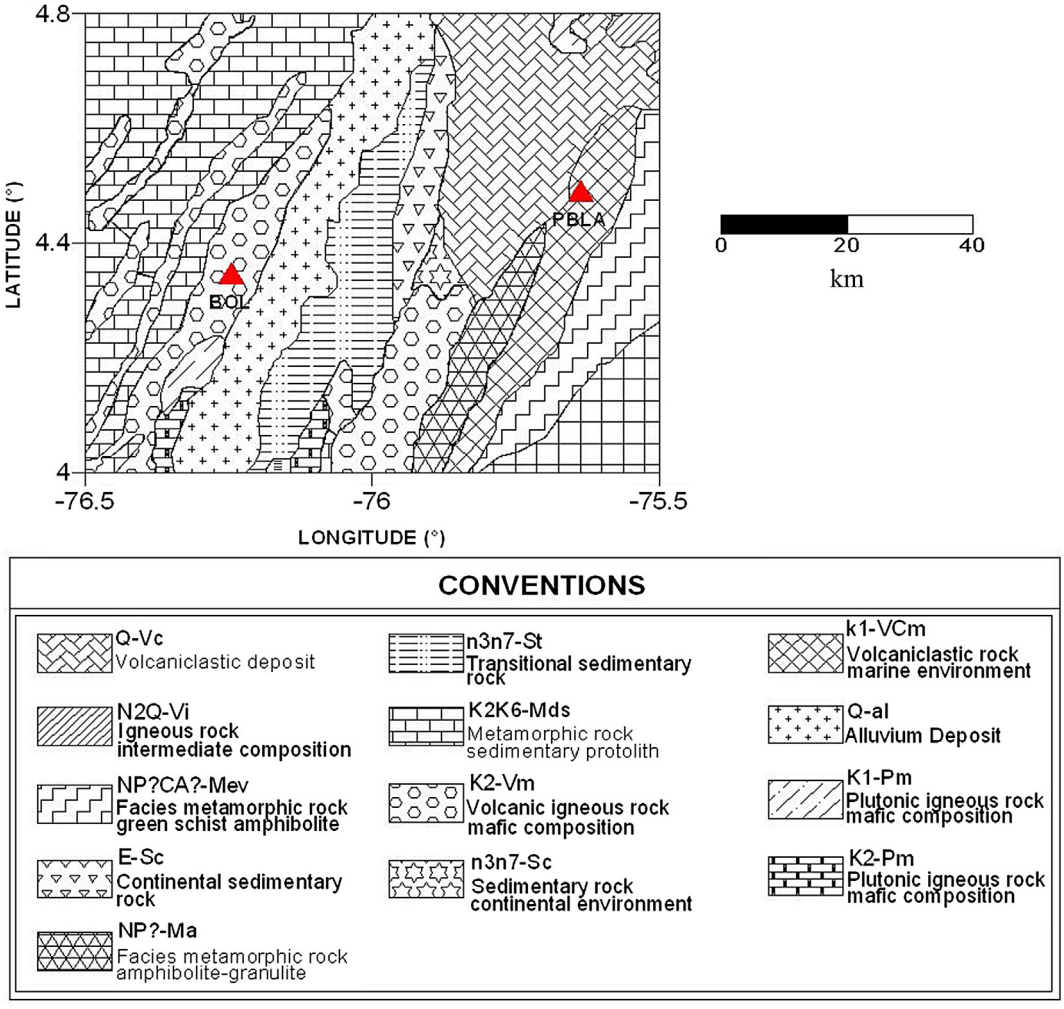

Fig. 2. Geologic map of the study zone. The red triangles show the location of the,seismic station BOL at the WC and the station PBLA at the CC. The convension for the geologic units is shown below (Modified from INGEOMINAS, 2007). (For interpretation of the references to color in this figure legend, the reader is referred to the web version of this article.)

Table 1
Location of the seismic stations BOL and PBLA, used in the calculation of the receiver functions.

Station	Code	Latitude(°) North	Longitude (°)West	Datum (AMSL)	Region
Bolivar	BOL	4.341	−76.246	3020	Regional Aqueduct BRUT
Peñas Blancas	PBLA	4.47925	−75.63173	2072	La Virginia

for the seismic traces were performed with the software SAC. All data files corresponding to three components (E, N, and Z) were collected in order to include information of the earthquakes and the stations, such as latitude, longitude, and depth; with this data input in SAC, the values of azimuth (AZ) and back-azimuth (BAZ) were calculated for the different seismic traces. The P-wave arrival is identified and marked in the vertical component of each seismogram, and then, with this mark, the first arrival is picked in the other two horizontal components. It was also necessary to perform baseline correction. Afterwards, the horizontal components (EW, NS) were rotated in order to obtain the radial and tangential components respectively (R y T), by aligning the ray with radial component through the rotation of the back-azimuth. The next step consisted of changing the sampling rate of the pre-selected signals, in all components.

3.3. Grouping of earthquakes epicenters

Earthquake epicenters were plotted on a map so that they could be grouped by visual inspection. The minimum number of earthquakes per group was agreed to be three, comprising thus two groups for station BOL and three groups for station PBLA. For station BOL these groups were labeled Alaska and Sandwich respectively and for station PBLA these groups were labeled Aleutian, California, and Sandwich respectively (see Fig. 3, also Tables 2 and 3).

The idea of collecting the seismic events into groups within a limited range of back-azimuth to stack all receiver functions is done to avoid significant changes of the incident angles that may result in undesirable variations due to the travel path. Stacking the functions suppresses the noise and accentuates the most important seismic phases.

4. Analysis of receiver functions

When teleseismic waves arrive at a seismic station, they contain information from the path they have gone through along their trip. As a result, the recorded seismic data contains information about the seismic source, the propagation path through the mantle and the local structure beneath the seismic station. Receiver function analysis is a method that removes information from seismic traces such as source structure effects and propagating path effects so that the resulting data set only contains information about the local structure beneath the seismic station; this data set is called the receiver function, which is a spectral ratio obtained from teleseismic earthquakes recorded by broadband seismic stations. This methodology is based on the fact that P waves impinging on a subsurface boundary will result in refracted and reflected P and S-waves which are only the result of the local structure and by deconvolution the local effect can be isolated. This is done by reconstructing the local velocity-structure via the comparison of the observed receiver functions with synthetically generated receiver functions (see Fig. 4).

4.1. Global optimization algorithms

Several authors have shown that receiver functions are sensitive to discontinuities in the distribution of effects caused by changes in the absolute value of wave velocities and the thickness of the crustal layers, but the trade-off between the velocity and the thickness of the layers can occur in such a manner that it produces non-unique solutions (Cruz, 2000). The opposite occurs in the dispersion curves of surface waves (Love and Rayleigh), where group and phase velocities are much more sensitive to the absolute value of wave velocities than to the presence of discontinuities; that is, the parameters are decoupled and the solution is unique.

This suggests two possible solutions to better constrain the non-uniqueness of the solution for the velocity structure model: a joint inversion with surface waves or the possibility of covering the "whole" sample space (a huge amount of possible models) using a random process that can be combined with other initial models along with a genetic algorithm (GA) and a simulated annealing algorithm (SA).

4.1.1. Genetic algorithm (GA)

Genetic algorithm is a heuristic search process used in computational sciences and artificial intelligence. It works analogously to natural evolution and are used for useful solutions to optimization problems in different fields of science and engineering. An initial population is established, each of them represents a factual solution to the given problem. Each of the individuals of this population is given a fitting grade which represents the effectiveness of the solution. Comparing this to what happens in natural life would be similar to the ability of an organism to compete for specific available resources. The next generation of individuals is created by selection, mutation, inheritance or crossover and it is supposed to be superior to the previous one. The selection of the parents is done randomly using a procedure that favors the best fitting individuals. Since each individual is assigned a probability to be chosen which is proportional to its adapting function, it will define the parents for the next generations. The population will evolve through ensuing generations and therefore the mean adaptation will be passed to the individuals of the population, thus the ability to adapt of an individual will increase until reaching an optimal value.

4.1.2. Simulated annealing (SA)

Simulated annealing is a process that is based on energy changes in a system of particles where the temperature decreases; this process then is carried out until the system reaches a steady state (cooling). Simulated annealing was proposed by Metropolis et al. (1953) and was initially applied to the field of statistical thermodynamics. Laws of thermodynamics say that for a given temperature t, the probability of experiencing an energy increment can be approximated by:

$$P[\delta E] = \exp(-\delta E/kt) \quad (1)$$

where k is a physical constant known as Boltzmann constant. In the algorithm proposed by Metropolis a random perturbation is generated within the system and the resulting energy changes are calculated: If there is an energy decrease, this change is taken automatically; on the contrary, if there is an energy increase, this change will be taken with a probability given by $P[\delta E] = \exp(-\delta E/kt)$. This process is repeated iteratively for decreasing temperatures until the system is cold. Boltzmann constant here is not considered since it does not have any meaning in optimization problems. This idea of slow cooling is implemented in the Simulated Annealing algorithm as a slow decrease in the probability of accepting worse solutions as it explores the solution space (Laarhoven and Aarts, 1989).

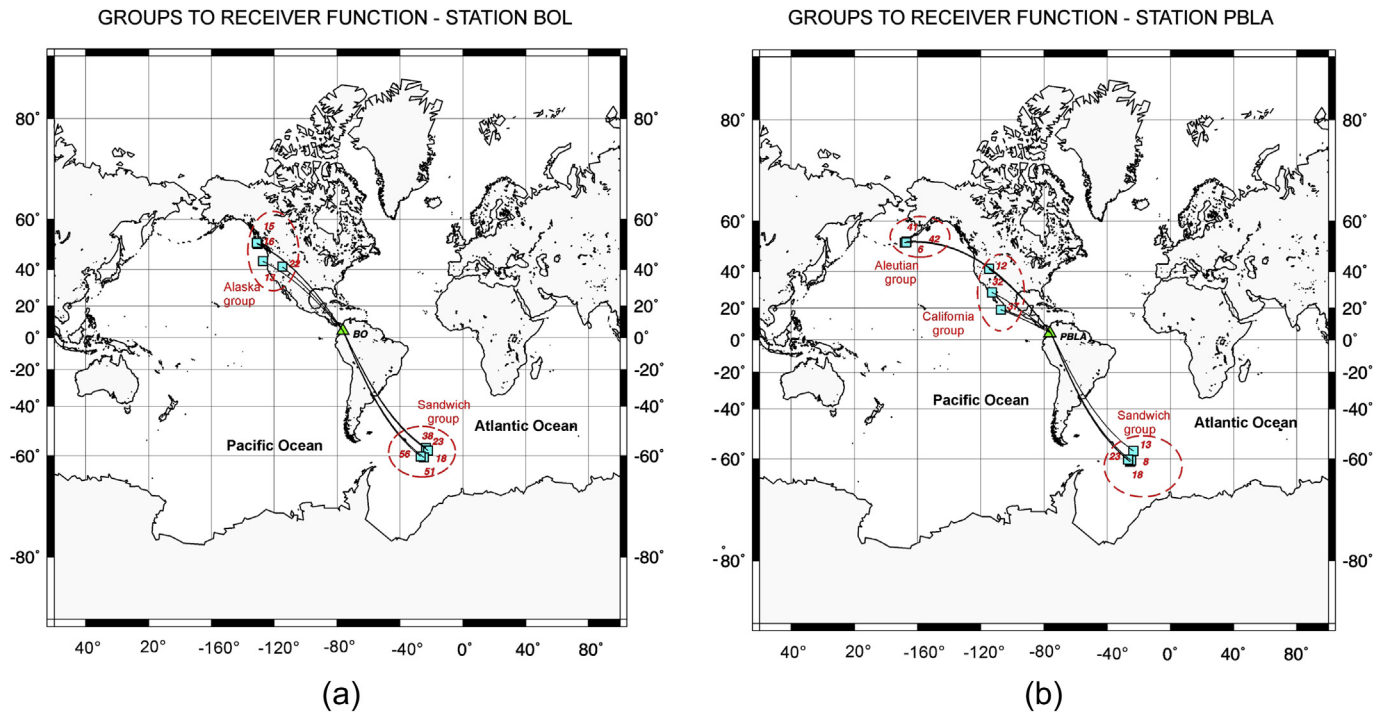

Fig. 3. a) 81 Selected teleseismic earthquakes, at distances Δ ranging between 30° and 90° (blue squares), recorded at the station BOL (green triangles). b) 45 Selected teleseismic earthquakes, at distances Δ within 30° and 90° (blue squares), recorded at the station PBLA (green triangles). Red circles show the groups used for receiver function analysis. (For interpretation of the references to color in this figure legend, the reader is referred to the web version of this article.)

Morales (2010) developed two global optimization algorithms implemented in this work to select models from the different groups by global optimization. In the algorithms three selection criteria were established in order to obtain elitist models. The first criterion was the best fit or mean quadratic error between synthetic and observed receiver functions obtained using the software for the inversion of the receiver functions. The second criterion consisted of obtaining the semblance between the receiver functions through the following equation:

$$S(m) = 0.5 - \frac{xcorr(F.ob \cdot F.syn)}{xcorr(F.ob) + xcorr(F.syn)} \quad (2)$$

Where ***m*** is the number of models to be tested, ***S*(*m*)** is the score given to the semblance of each model, ***F.ob*** is the stacking of the observed receiver functions, ***F.syn*** is the synthetic receiver function, ***xcorr* (*F.ob*)** is the autocorrelation of the observed receiver function, and ***xcorr* (*F.syn*)** is the autocorrelation of the synthetic receiver function. ***xcorr* (*F.ob, F.syn*)** gives the cross-correlation between ***F.ob and F.syn.***

The third selection criterion, called area of error, consisted of calculating how much area of the receiver function curve is outside the area bounded by the stacking of the observed receiver functions plus and minus one standard deviation as shown in Fig. 5. Therefore, the area between the stacking of the observed receiver functions plus and minus one standard deviation has to be computed; this area is referred to as total area (A_t). After having A_t, the area of the synthetic receiver function that is outside the boundary established by the stacking of the observed receiver functions plus and minus one standard deviation must be computed. This ensued calculated area is called deviated area (A_d). Using A_t and A_d the area of error A_E is calculated as follow:

$$A_E = \frac{A_d}{A_t} \quad (3)$$

This area of error assigns a score for the fitting in order to validate the elitist models.

4.2. Synthetic model

To verify the performance of the global optimization algorithm, a one-layer model over a halfspace was used (Table 4). Based on this

Table 2
Earthquake events grouped in the seismological station BOLIVAR – BOL.

#	Latitude	Longitude	Magnitude	Depth	Δ (km)	AAMMDDHHMMSS	Ray
			Mw	km			s/km
Sandwich group							
18	−60.80	−25.59	6.6	8.0	75.93	080210122202	0.05136
23	−57.33	−23.42	6.7	10.0	74.80	080223155719	0.05211
38	−58.22	−22.10	7.0	19.0	75.88	081030151541	0.05138
56	−60.18	−26.84	6.7	20.0	75.07	090416145706	0.05192
Alaska group							
13	51.25	−130.75	6.6	15.0	65.06	080105110106	0.05853
15	51.65	−131.18	6.1	10.0	65.47	080109144000	0.05827
16	43.78	−127.26	6.3	13.0	59.63	080110013719	0.06209
22	41.15	−114.87	6.0	6.0	50.45	080221141602	0.06808

Table 3
Earthquake events grouped in the seismological station PBLA.

#	Latitude	Longitude	Magnitude	Depth	Δ (km)	AAMMDDHHMMSS	Ray
			Mw	km			s/km
Aleutianas group							
6	−168.22	52.56	6.4	25.0	88.05	071226220454	0.04258
41	−167.039	52.959	6.5	18.0	87.02	091013053722	0.04372
42	−167.21	52.657	6.4	22.7	87.09	091013202155	0.04357
California group							
32	−112.90	29.03	6.9	10.0	42.96	090803175956	0.07287
37	−107.36	18.98	6.3	37.0	34.17	090924071624	0.07383
12	−114.87	41.15	6.0	6.0	50.74	080221141602	0.07689
Sandwich group							
8	−25.59	−60.80	6.6	8.0	75.80	080210122202	0.05145
13	−23.42	−57.33	6.7	10.0	74.62	080223155719	0.05223
18	−24.75	−60.47	6.3	10.0	75.95	090228143305	0.05134
23	−26.84	−60.18	6.7	20.0	75.07	090416145706	0.05192

model, six receiver functions were estimated (Fig. 6) using different ray parameter, for an earthquake at a depth of 20, 33 and 96 km within a group at epicentral distance of ∼60°.

The synthetic receiver functions were added with random Gaussian noise and inversions were performed with two GA's. As shown in Fig. 6, the average models obtained with GA and SA fit well the target model. It can also be observed in Fig. 7 that models are more sensitive to the variation within the upper 10 km of the structure.

4.3. Station BOL

Most receiver functions have large radial amplitudes compared to the tangential amplitudes (Fig. 8); this suggests a significant impedance contrast beneath the station since there exists a strong agreement with the phases coming from similar azimuths. A phase arrival of negative amplitude at around 3–4 s after the arrival of the Pp phase is a feature that almost all radial receiver functions exhibit.

By the stacking of each one of the groups, a receiver function was obtained by averaging the depth as well as the epicentral distance, and then the ray parameter was calculated for the stacked function. The radial function of BOL has large amplitudes compared to that of the transverse function; also, it could be noticed that the

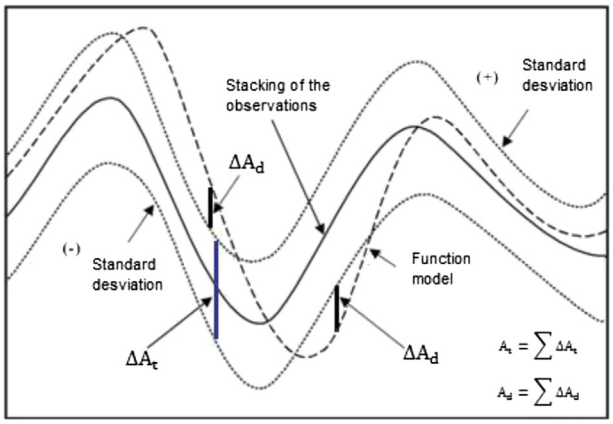

Fig. 5. The solid thick line shows the observed receiver function. The gray solid line shows the observed plus and minus one standard deviation respectively. The dashed line shows the synthetic receiver function obtained through inversion. Modified from Morales (2010).].

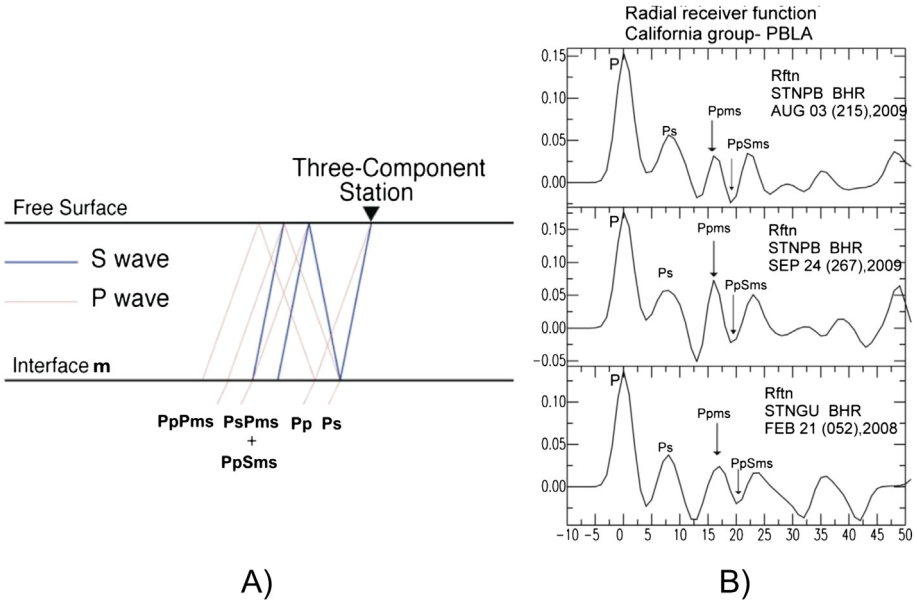

Fig. 4. A) Representation o seismic rays trapped in the crustal waveguide. B) Receiver function of the radial component in station PBLA, where P, Ps, Ppms, PpSms phases can be identified.

Table 4
One-layer model.

Layer	Depth (km.)	P wave velocity (km/s)
1	0–30	6.0
Halfspace		8.0

waveforms grouped by azimuth and distance show strong similarities (Fig. 9).

The difference in amplitude between the phase arrivals suggests a difference in the crustal structure. From the inversion of Alaska group, as shown in the Fig. 8A and B, a strong velocity gradient resulted in the upper 5 km as well as a low velocity layer between 15 and 20 km which corresponds to the upper crust; furthermore, there is a negative gradient between 20- and 40 km, which corresponds to the lower crust. In this work, as suggested by different authors (Owens et al., 1984; Ammon and Zandt, 1993; Mangino et al., 1993), the functions were stacked according to the ray parameter and the back-azimuth with the aim of reducing the noise due to dispersion.

100 models from the final data generation of GA and 100 models for SA may be seen in Fig. 9; the results of the inversion are plotted in solid lines. The sample space obtained using the two selection criteria previously mentioned is shown in different intensities of gray color; the fitting and resemblance were adjusted for all the

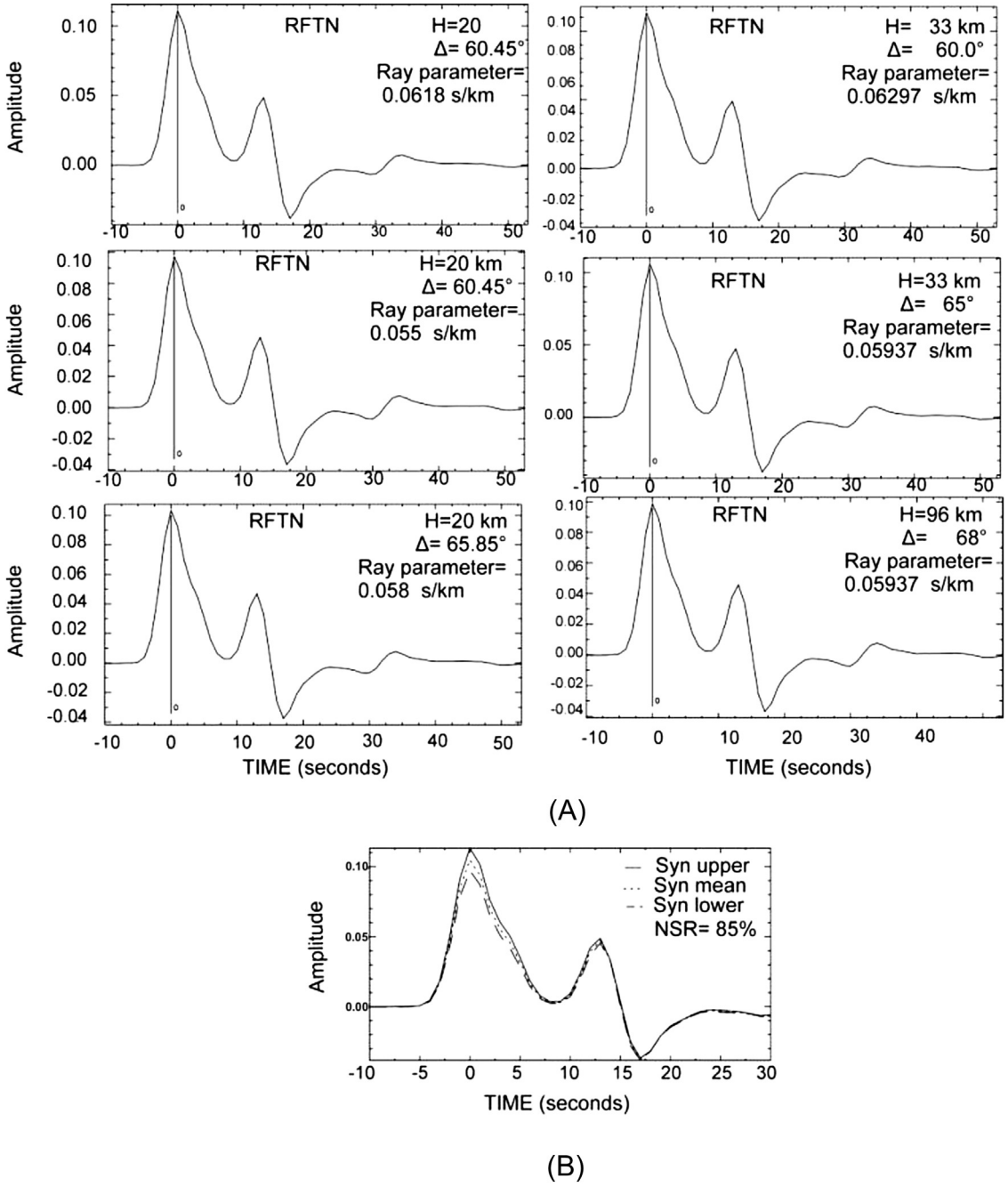

Fig. 6. A) Synthetic receiver functions with added noise, having signal-to-noise ratio (SNR) of 85%. This was performed over a group of six earthquakes with focal depths of 20, 33, and 96 km and six different ray parameters. B) Stacking of six receiver functions plus and minus one standard deviation.

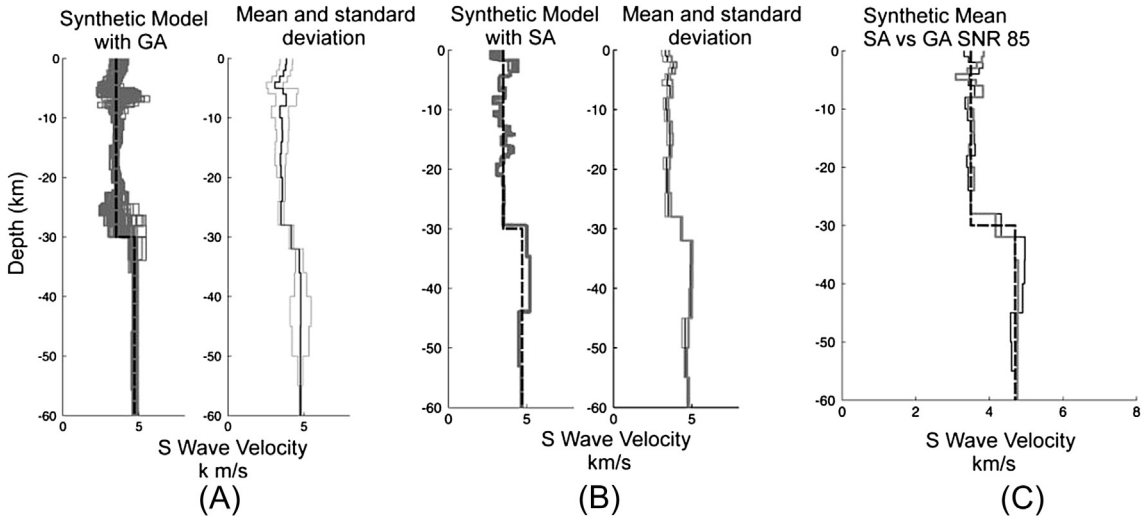

Fig. 7. Inversion using six receiver functions with added noise, having an SNR of 85%. A) The target model is shown in dashed line. Gray lines show the final 100 elitist models obtained by GA. In solid line the average model is shown with its respective standard deviation (Right). B) The target model is shown in dashed line. Gray lines show the final 100 elitist models obtained by SA. In solid line the average model is shown with its respective standard deviation (Right). C). The average model is shown in solid line while the target model is shown in dashed line.

mutated generation. A low velocity zone is observed between 15 and 20 km, which corresponds to the strong negative gradient between 2 and 3 s of the receiver functions.

The results of GA and SA are based on the selection criteria of the elitist models from the last generation of data that resulted after their acceptance criteria were met (Fig. 9). Initial and final ranges for the three selection criteria were established and met by the models shown in Tables 5 and 6 respectively. Fig. 9E shows the average models using GA and SA, whereas Vs values with their respective standard deviations are shown in Table 7.

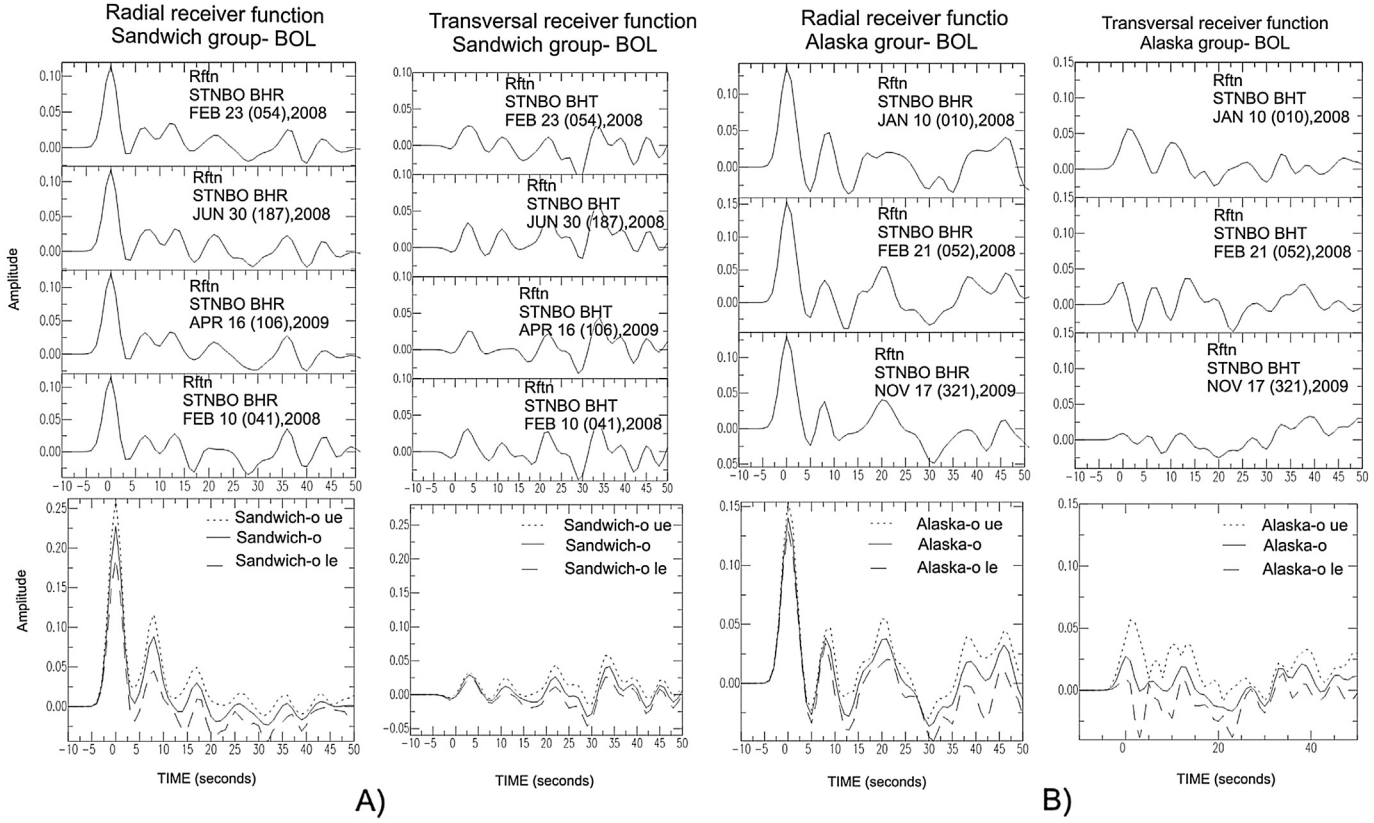

Fig. 8. Receiver functions of the station BOL for each group. Radial functions are shown to the left and transverse functions are shown to the right (both at scale). At the lower left, the stacking of radial functions plus one standard deviation is shown while the stacking of transverse functions plus one standard deviation are shown at the lower right. All the functions are at the same scale in order to compare the amplitude of both the transverse and radial functions. A) Sandwich Group, B) Alaska Group.

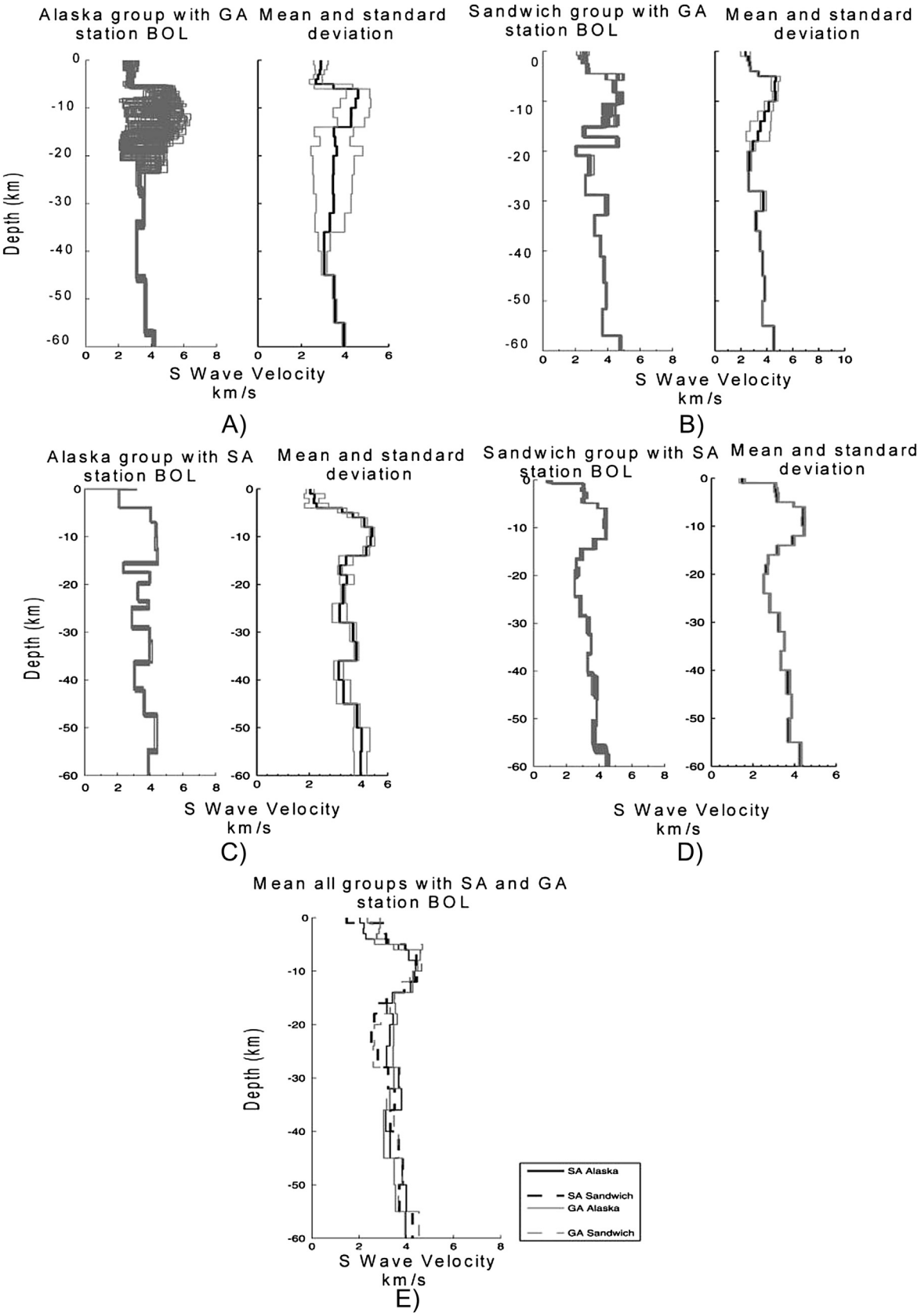

Fig. 9. Final 100 velocity structure models obtained from12,000 models using GA and from 10,000 models using SA in each group at BOL station. The average model is shown on the right in solid line whereas the average model ± a standard deviation is shown in gray line. A) Alaska group using GA. B) Sandwich group using GA. C) Alaska group using SA. D) Sandwich group using SA. E) Average models of all groups using both GA and SA.

Table 5
Initial and final values obtained with the selection criteria for the two groups of the BOL station using GA.

Fitting	Semblance	Area of error	Fitting	Semblance	Area of error
Alaska group			Sandwich group		
Input			Input		
92.04	0.031	0.076	94.08	0.021	0.12
Output			Output		
94.64	0.018	0.059	95.74	0.016	0.08

1-D velocity models were determined through linearized inversion in the time domain using the procedure by Ammon et al. (1990). Velocity structure models below each station were calculated using a combination of the inversion of random models obtained with GA and SA (Morales, 2010). Initial models were used as parents in GA; these models were parameterized as 1 and 2 km-thick horizontal layers within the first 20 km of depth; alternatively 5 and 10 km-thick horizontal layers were used between 20 and 60 km of depth. S-wave velocity was chosen as the free parameter in the inversion.

Fig. 10A shows two models of a single layer over a halfspace. The first one, in solid line, presents a 30 km-thick layer while the second model, in dashed line, presents a 40 km-thick layer, both having a P-wave velocity of 6.0 km.s-1 over a halfspace with a P-wave velocity of 8.0 km.s-1. Fig. 10B shows Ps phase arrival with a one-second delay indicated by the vertical lines. This difference observed in the receiver functions represents the travel-time arrival at the station of the phases Pp and Ps through which Moho depth can be inferred (one depth at 30 km and another at 40 km). The red circle on Fig. 10B indicates a pulse in the dashed line plot.

It can also be seen how the phase PsPms located at 17.5 s in the solid line plot moves to 20.5 s in the dashed line plot. This is interpreted as a variation of the layer thickness which causes a shift in the most important phases in the receiver function. In Fig. 10C there are two models: a one-layer model and another model with a low velocity zone. Fig. 10D exhibits the effect that a low velocity zone on the upper layers has on the receiver function; the red circle on Fig. 10D indicates a inverted pulse of the Pp phase, in the dashed line plot, that reaches a negative value in the receiver function amplitude. This negative value of the Pp phase is evidence of the low velocity zone, which is located between 10 and 15 km. The Moho boundary is located here at 30 km. There is a greater shift of the PsPms phase due to the fact that its travel-time is longer. Fig. 10E shows a single-layer model (Vp = 6.06 km s^{-1}) in solid line and a two-layer model (Vp = 6.06 km.s-1 and 6.92 km s^{-1}) in dashed line, both with the Moho boundary being located at 30 km. Fig. 10F shows in dashed line that the inverted pulse of the Pp phase (within the red circle) is wider and does not reach a negative amplitude, compared to the Pp phase on Fig. 10D. The fact that it does not exhibit negative amplitude can be interpreted as not having a low velocity zone below the first layer; that is, the velocity of the first layer is observed in the Ps phase arrival and, when there is a low velocity layer, the amplitude of the Pp phase goes further down and reaches negative values of amplitude.

A simple velocity structure can be used to model the main characteristics of the WC at station BOL. The upper 5 km exhibit a strong positive velocity gradient and the waveform agrees well with a low velocity zone between 5 and 20 km. The depth of the Moho (40 km) is inferred by the first 20 s of the Pp phase arrival as shown in Fig. 8. Fig. 11 shows average models with both GA and SA. The dashed line shows the final model within plus and minus one standard deviation. Table 6 summarizes the final results. The final models obtained using GA and SA are shown in Table 8, which correspond to an inferred mean model plus and minus one standard deviation.

Table 6
Initial and final values obtained with the selection criteria for the two groups of the BOL station using SA.

Fitting	Semblance	Area of error	Fitting	Semblance	Area of error
Alaska group			Sandwich group		
Input			Input		
93.01	0.023	0.09	93.89	0.025	0.06
Output			Output		
94.31	0.016	0.016	95.53	0.017	0.02

4.4. Station PBLA

Analogously to what was observed at station BOL, most receiver functions in station PBLA have large radial amplitudes compared to tangential amplitudes which also suggests a significant impedance contrast beneath the station. Also, there is a strong agreement between the phase arrivals from similar azimuths.

A negative pulse of the receiver function between 3 and 4 s after the arrival of the PpPms phase is shown; this pattern is observed in almost all radial receiver functions. Similarly, a shift of 0.5 and 1.0 s from the origin is observed in the arrival of the Pp phase for the functions of Sandwich group at station PBLA (Fig. 12).

The crustal structure beneath station PBLA was obtained from 10 inverted receiver functions; these receiver functions were calculated with seismic events from different azimuths. At depths between 2 and 3 km there is a strong velocity gradient of about 2.8 km s^{-1}. Below this gradient, there is a modest negative velocity gradient in Aleutian group that extends to a depth of 20 km beneath Aleutians group and 30 km beneath Sandwich and California groups respectively. This negative gradient is estimated from a moderate arrival of a negative amplitude pulse between 3 and 4 s below 15 km; there is a positive velocity gradient that corresponds

Table 7
Velocity structure model beneath BOL station. Average model obtained from 100 elitist models with GA and SA; and overall average model.

Station BOL			
Thickness	Mean model GA	Mean model SA	Joint mean model SA + GA
H (km)	VS (km/s) ± deviation	VS (km/s) ± deviation	VS (km/s) ± deviation
1	2.6251 ± 0.3490	1.7603 ± 0.1396	2.1783 ± 0.2443
1	2.7385 ± 0.2109	2.6326 ± 0.2287	2.5848 ± 0.2198
1	2.7623 ± 0.1551	2.6416 ± 0.1415	2.7924 ± 0.1483
1	2.7506 ± 0.1317	2.7163 ± 0.2765	2.9045 ± 0.2041
1	3.0109 ± 0.1908	3.2120 ± 0.1207	3.1302 ± 0.1558
1	4.0789 ± 0.6138	3.8135 ± 0.1217	3.8831 ± 0.3677
2	4.6023 ± 0.4087	4.2675 ± 0.0927	4.1618 ± 0.2507
2	4.5661 ± 0.4518	4.4069 ± 0.0874	4.1268 ± 0.2696
2	4.2186 ± 0.5876	4.3995 ± 0.1013	3.9797 ± 0.3444
2	4.0473 ± 0.5702	4.0510 ± 0.1008	3.9459 ± 0.3355
2	3.4986 ± 0.8479	3.2913 ± 0.1713	3.7133 ± 0.5096
2	3.4293 ± 0.7972	2.9518 ± 0.0632	3.6873 ± 0.4302
2	3.2722 ± 1.0692	3.0432 ± 0.1797	3.5595 ± 0.6244
4	3.0601 ± 0.5595	2.9118 ± 0.0518	3.2693 ± 0.3056
4	3.0230 ± 0.4777	2.9822 ± 0.1670	3.0443 ± 0.3223
4	3.6041 ± 0.5081	3.4588 ± 0.0958	3.3529 ± 0.3019
4	3.2374 ± 0.3998	3.6545 ± 0.0535	3.2908 ± 0.2266
4	3.2627 ± 0.1799	3.2290 ± 0.1077	3.3670 ± 0.1438
5	3.3621 ± 0.1035	3.4982 ± 0.1858	3.5059 ± 0.1447
5	3.6634 ± 0.0756	3.8390 ± 0.0669	3.7417 ± 0.0713
5	3.6064 ± 0.0697	3.8565 ± 0.1994	3.6752 ± 0.1345
5	4.2419 ± 0.0849	4.1165 ± 0.1538	3.9132 ± 0.1193
5	4.4386 ± 0.0746	4.3778 ± 0.0842	3.9867 ± 0.0794

to a velocity of 3.4 km s^{-1} at a depth of 20 km. Below 43 km, the model is represented by a simple halfspace.

100 elitist models from the last generation of data using GA and 100 elitist models using SA are shown in Fig. 13; the results of the inversion are plotted in solid lines. The sample space obtained using the two selection criteria is shown in different intensities of gray color; the fitting and resemblance were adjusted for all the mutated generation. Fig. 13 also shows that the three groups exhibit a subtle variation in the average model for each group. This suggests lateral variations within the crustal structure. The crustal structure of the CC, beneath the station PBLA, reveals a small negative velocity gradient in Aleutian group, which extends to 20 km deep; this gradient extends to 30 km deep in both Sandwich and California groups.

The results of the GA and SA are based on the selection criteria of the elitist models from the last generation of data that met the acceptance criteria. Initial and final values obtained using GA and SA are shown in Tables 9 and 10 respectively. Fig. 13G shows the average models using GA and SA, whereas the Vs values with their respective standard deviations are shown in Table 11.

A simple structure, as shown in Fig. 14, can model the main characteristics of the CC; the first 6 km exhibit a modest positive velocity gradient whereas a slight negative velocity gradient is present between 6 and 18 km. The Moho boundary was found at a

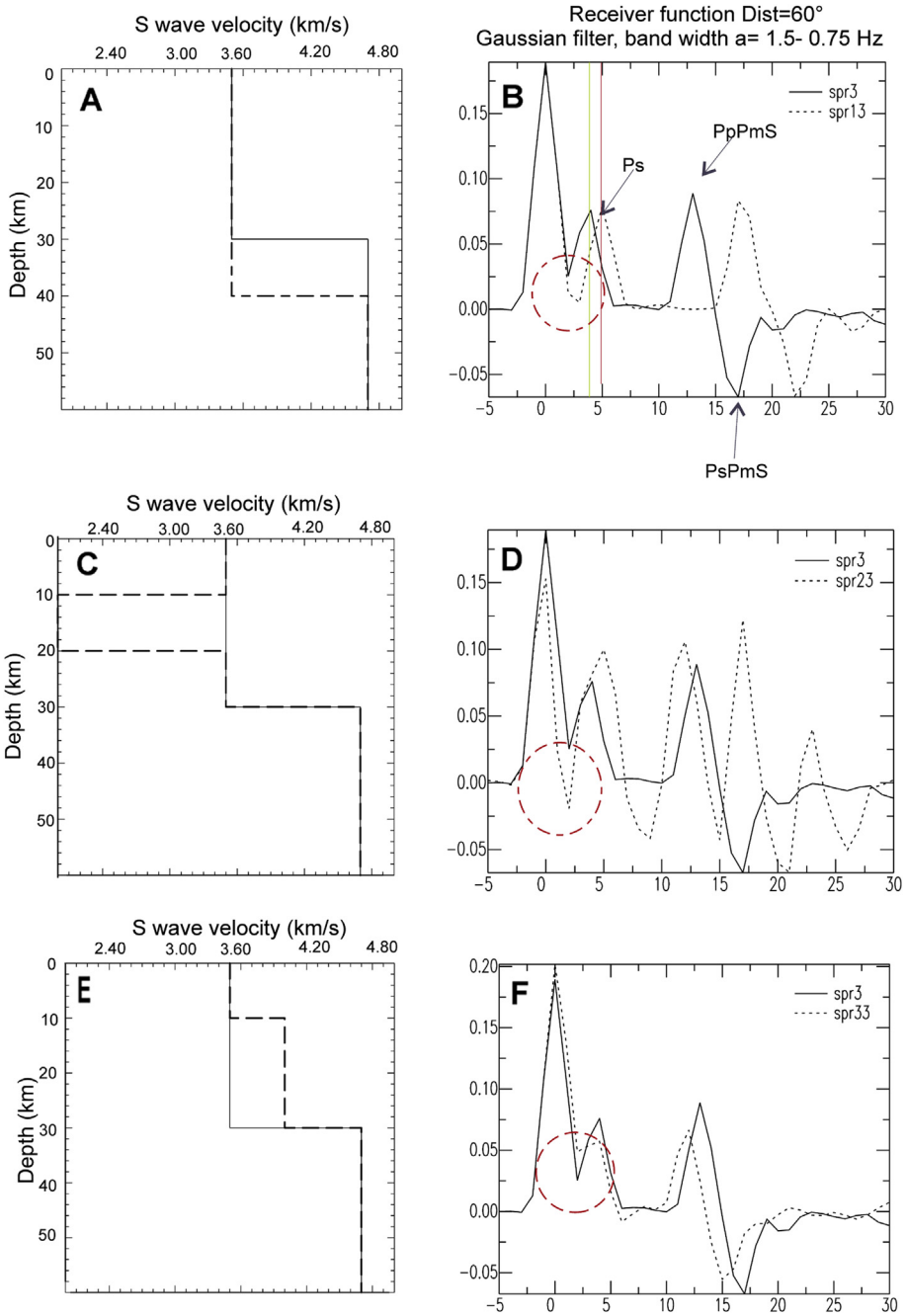

Fig. 10. Synthetic modeling of receiver functions for one and two layer velocity structure. Distance 60°, ray parameter 0.0618 and Gaussian filter a = 1.5, 0.75 Hz. A), C) and E) correspond to S-wave velocity models tested; B), D) and F) represent the respective receiver functions.

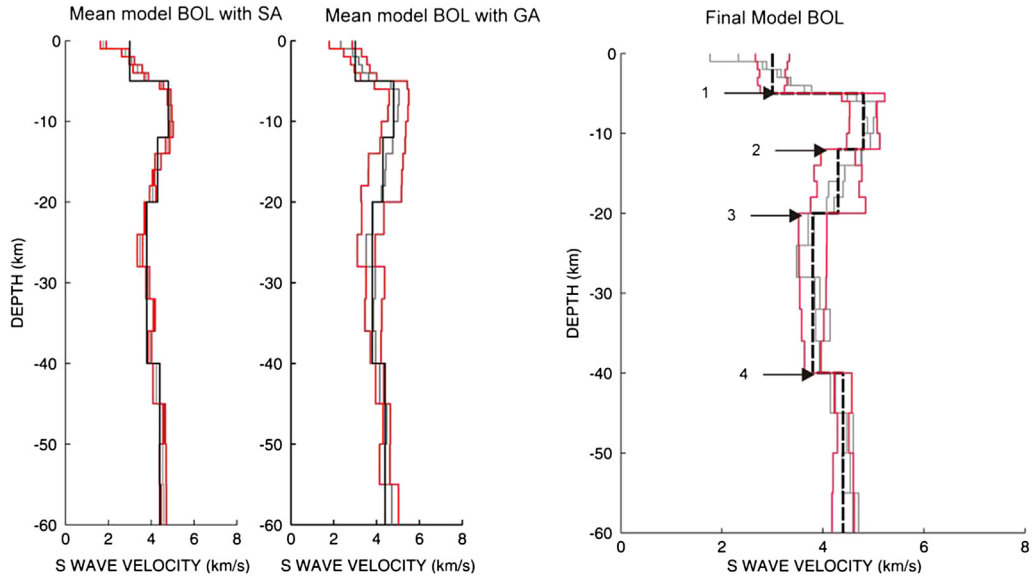

Fig. 11. The left plot shows the average structure model beneath BOL station within a standard deviation using SA. The central plot shows the average model beneath BOL station within a standard deviation using GA. The right plot shows the final velocity structure model in dashed line for the WC obtained beneath BOL station with the inversion of 48,000 models using GA and 40,000 models using SA. Four layers are shown over the Moho boundary, which is located at 40 km, for the final model. Gray lines show the average using SA and GA plus and minus one standard deviation. The locations labeled 1, 2 and 3 show the most significant variations.

depth of 43 km. The depth of the Moho agrees with the 20 s of the PpPms phase arrival.

The waveforms grouped by azimuth and distance show strong similarities. The difference in amplitude between the arrivals suggests a difference in the crustal structure. From the inversion of Aleutian group, a strong velocity gradient was found in the upper 5 km and a low velocity layer was also found between 15 and 25 km, which is located in the upper crust; also there is a positive gradient between 30 and 60 km, which is located in the lower crust.

Contrast at the Moho is clearly related to the arrival of the phase Ps, this allowed to estimate the Moho boundary at 43 km. S wave velocity reaches up to 3.8 km s^{-1} between 6 and 18 km. The model obtained from California group has a similar behavior. The high velocity of the structure at 43 km matches well the multiple arrivals (between 20 and 25 s) after the Pp phase has arrived.

The results suggest a model with an upper crust, between 6 and 18 km, with a velocity of 3.8 km s^{-1} and a strong positive velocity gradient. At 4 s, a large negative pulse in the receiver function is identified as well as a low velocity zone between 18 and 40 km. A simple structure can model the main characteristics of the WC; the upper 5 km exhibit a strong positive velocity gradient, and the waveform agrees with the low velocity zone between 10 and 25 km and a Moho boundary at 43 km. The Moho thickness is obtained within the first 20 s of the Pp phase arrival, as shown in Fig. 14. Table 11 shows the final model.

5. Discussion

The receiver function technique are broadly used to study lithospheric structure and discontinuities in the upper mantle, especially in subduction zones since this method allows to retrieve information about the velocity contrast in such complex areas. The algorithm developed by Herrmann and Ammon (2002) does not consider lateral heterogeneities in the crust, nor anisotropy in the mantle; this may explain variations in the receiver functions for different azimuth. This occurs, for instance, in station PBLA for Sandwich group and the reason could be anisotropy in the upper mantle or crustal heterogeneities beneath the station. Silver (1996) found that anisotropy in the mantle is highly influenced by the crystalline structure of olivine. The seismic rays that travel through the mantle are affected by this anomalies as well as the dipping angle of the subducting plate.

Table 8
Final Model for the WC beneath BOL station.

Layer	Depth (KM)	Vs (km/s)	Vp (km/s)	Density (g/cm^3)
1	0–5	3.00 ± 0.31	5.31	2.47
2	5–12	4.80 ± 0.38	8.50	3.49
3	12–20	4.30 ± 0.24	7.61	3.21
4	20–40	3.80 ± 0.24	6.73	2.92
5	40–60	4.4 ± 0.16	7.79	3.26

The results described herein are average inversions of the receiver functions for each one of the broadband seismic stations. The fact that the solution of the inversion is not unique was taken with care regarding the GA that covers a broad sample space in the crust using approximately 48,000 random models for each station in order to constrain better the most reliable models. Five models obtained in regional studies have been part of the mutation, crossover, and selection process. In the results shown in Figs. 11 and 14, the two stations show different depths for the Moho. The effectiveness of the receiver functions to constrain the S-wave velocity structure depends on the level of noise in the functions.

The results of the analysis of receiver functions suggest that the crustal structure of the CC has a thickness of 43 km whereas the thickness of the surface layer goes from 2- to 3 km the obtained velocity structure profiles show an increase of the velocity gradient. Above the Moho discontinuity, the S-wave velocity is between 4.1 and 4.4 km s^{-1} and the density is between 2.82 and 3.09 g/cm^3.

The results of the structure at the WC vary up to a thickness of 40 km. The thickness of the surface layer is between 2 and 3 km while the density is of about 2.47 g/cm^3. The velocity and depth profiles show a low velocity zone between 12 and 20 km with a moderate velocity gradient. At the Moho boundary, the velocity is about 4.4 km s^{-1}.

5.1. Low velocity zone

Below station BOL there is a moderate low velocity zone that cannot be attributed to high temperature fluids related to tectonic

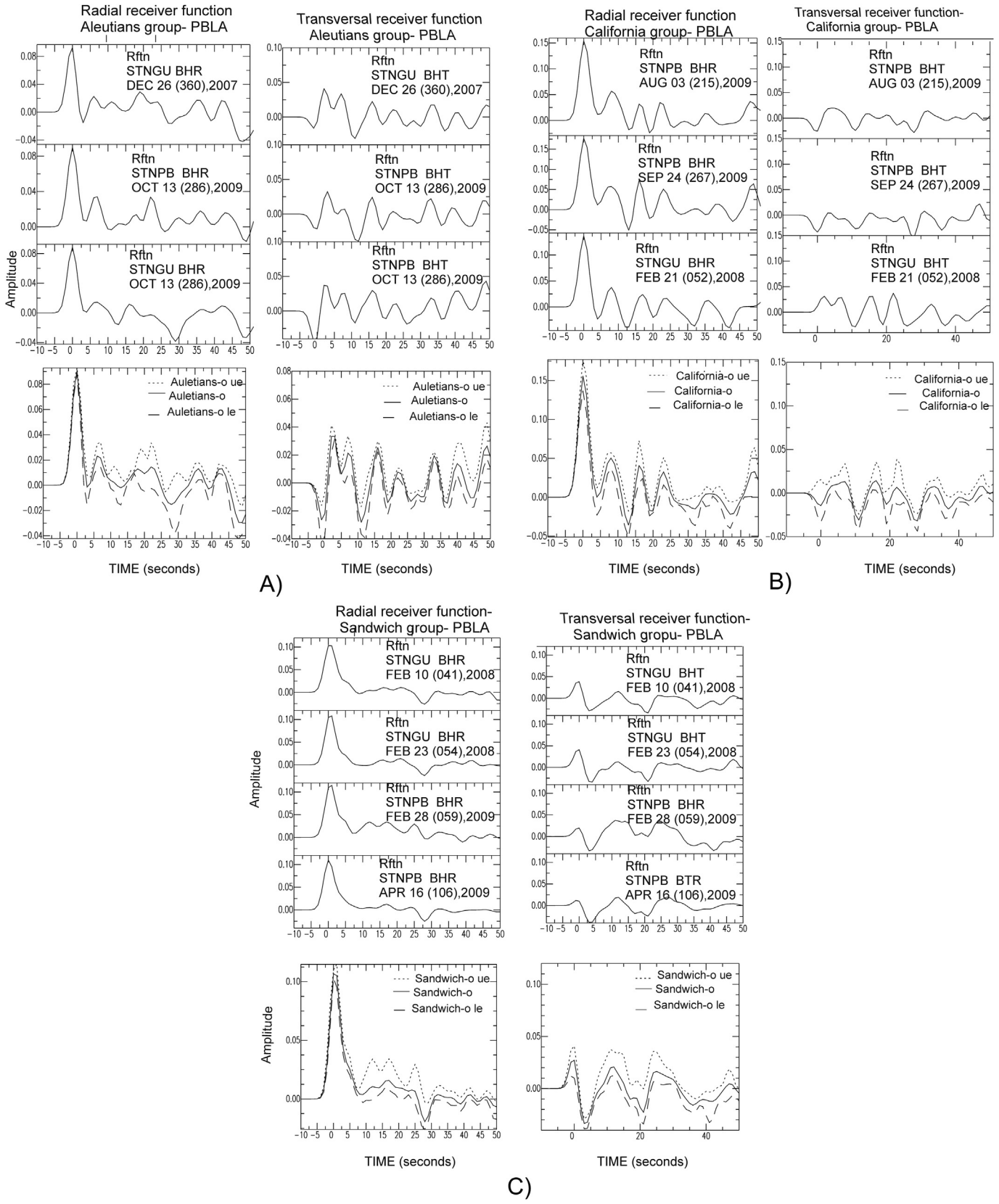

Fig. 12. Receiver functions of the station PBLA for each group. Radial functions are shown to the left and transverse functions are shown to the right (both at scale). At the lower left, the stacking of radial functions plus one standard deviation is shown while the stacking of transverse functions plus one standard deviation are shown at the lower right. All the functions are at the same scale in order to compare the amplitude of both the transverse and radial functions. A) Aleutian Group, B) California Group, C) Sandwich Group.

considerations, despite the existence of Bolivar ultramaphic complex and a group of basaltic rocks defined as Volcanic Formation by Nivia (1994), since there are not magma chambers. The presence of fluids is characterized by low velocities but high gradients; in contrast, this case exhibits a modest gradient. This might be due to the fact that the WC is composed of accretionary crust that exists over the continent, therefore it is constituted of highly folded rock and it could be logical to consider that in this zone there is fractured or weak rock due to this tectonic process. Besides, the receiver functions that are shown in Fig. 8 exhibit a prominent arrival of the Ps phase with negative amplitude between 3 and 4 s, which is coherent with the existence of a low velocity zone, as described in Fig. 12.

5.2. Comparison between the gravity model and the receiver function

Fig. 15 shows the profile obtained in the study area by Alexander et al. (2010), from gravity and magnetic joint inversion that corroborates a simple model of crustal structure showing a 6-km thick

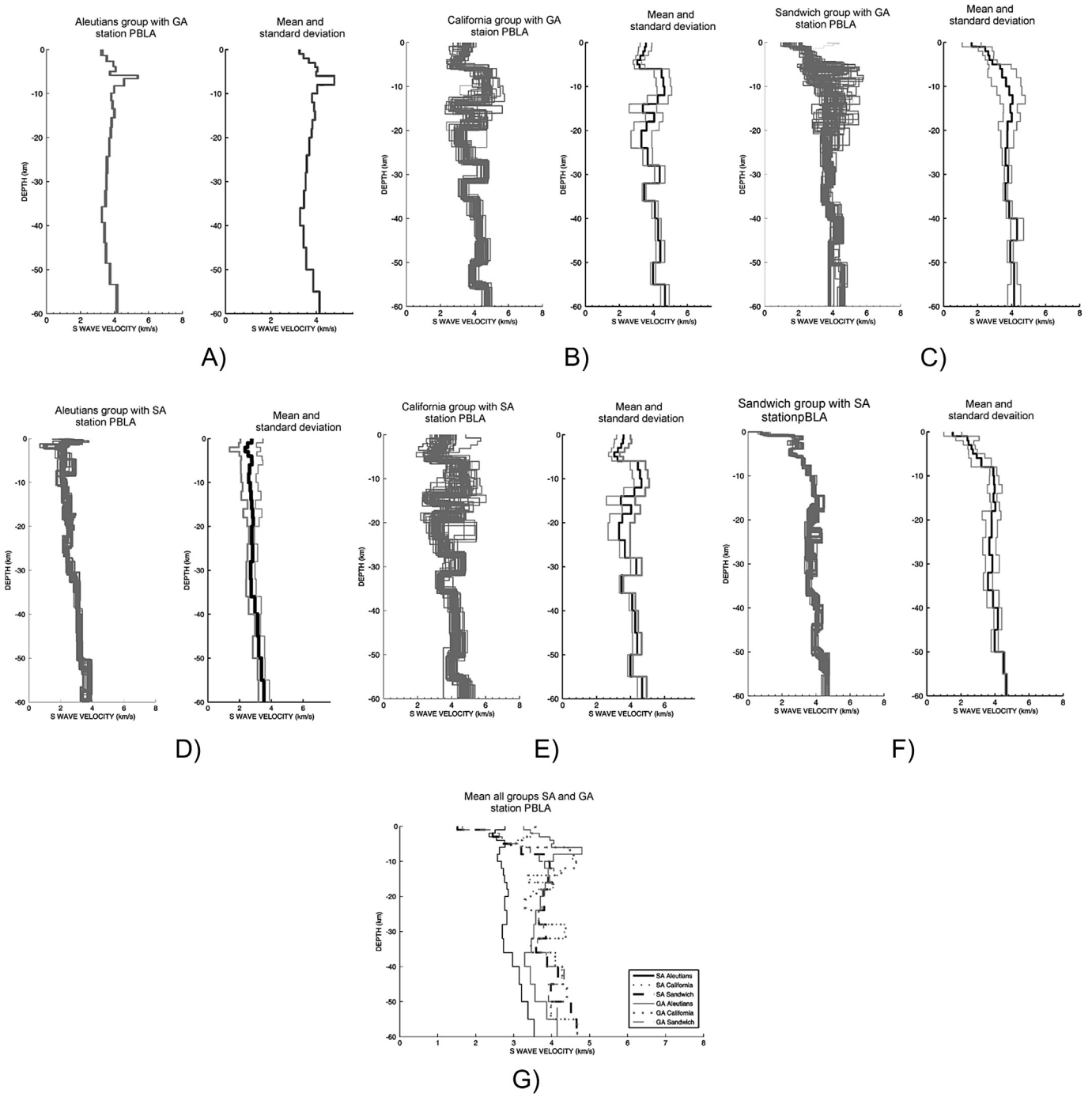

Fig. 13. Final 100 velocity structure models obtained from12,000 models using GA and from 10,000 models using SA in each group at PBLA station. The average model is shown to the right in solid line whereas the average model plus and minus a standard deviation is shown in gray line. A) Aleutian group using GA. B) California group using GA. C) Sandwich group using GA. D) Aleutian group using SA. E) California group using SA. F) Sandwich group using SA. G) Average models of all groups using both GA and SA.

Table 9
Initial and final values obtained with the selection criteria for the three groups of the PBLA station using GA.

Fitting	Semblance	Area of error	Fitting	Semblance	Area of error	Fitting	Semblance	Area of error
Aleutian group			California group			Sandwich group		
Input			Input			Input		
83.21	0.05	0.087	83.04	0.20	0.21	97.58	0.0435	0.543
Output			Output			Output		
85.87	0.041	0.065	86.96	0.14	0.14	98.06	0.043	0.046

Table 10
Initial and final values obtained with the selection criteria for the three groups of the PBLA station using SA.

Fitting	Semblance	Area of error	Fitting	Semblance	Area of error	Fitting	Semblance	Area of error
Aleutian group			California group			Sandwich group		
Input			Input			Input		
87.56	0.049	0.09	88.74	0.045	0.071	97.03	0.008	0.054
Output			Output			Output		
99.53	0.0036	0.073	90.31	0.027	0.051	98.48	0.0050	0.046

Table 11
Velocity model beneath PBLA station. Average models obtained from the final 100 elitist models using both GA and SA are shown as well as the overall average model.

Layer	Depth (KM)	Vs (km/s)	Vp (km/s)	Density (g/cm^3)
1	0–6	3.00 ± 0.37	5.31	2.47
2	6–18	3.80 ± 0.44	6.73	2.92
3	18–40	3.40 ± 0.25	6.02	2.70
4	40–60	4.10 ± 0.17	7.26	3.09

surface crust overlying a stronger layer of rock with a noticeable velocity change. The P wave velocity was obtained from the ratio Vp/Vs = 1.77 which was calculated by (Florez and Osorio, 2010). An obvious variation of the Moho boundary at 60, 43, and 36 km is observed in Fig. 15; furthermore, there are two layers between 20 and 25 km that contour the upper and lower crust.

Regarding the density, in station BOL, there are higher values than the obtained in the gravity model, especially the zone from 6- to 15 km which correspond to the upper crust. In station PBLA, there are greater density values in both the upper and lower crust; this suggests a difference in P-wave velocity between the two previously mentioned layers.

5.3. Comparing local and regional geology

The CC is mainly composed of plutonic and metamorphic rocks coated by isolated remnants of marine sedimentary rocks. Different techniques provide a better resolution for the crustal structure and this has prompted the creation of database at a worldwide level. The results of this database have been validated by testing for a considerable group of rocks within the crust (Christensen and Mooney, 1995), and for the particular case of the Andes, the wave velocities obtained are listed in Table 12.

Comparing the metamorphic rocks of the Precambrian and Paleozoic age, sandstones and green rocks, cataclastic schists, serpentine rocks, granodiorites and diorites from the cretaceous period in the CC with the wave velocities obtained by Christensen and Mooney (1995) in the Andes at different depths (Table 12), it

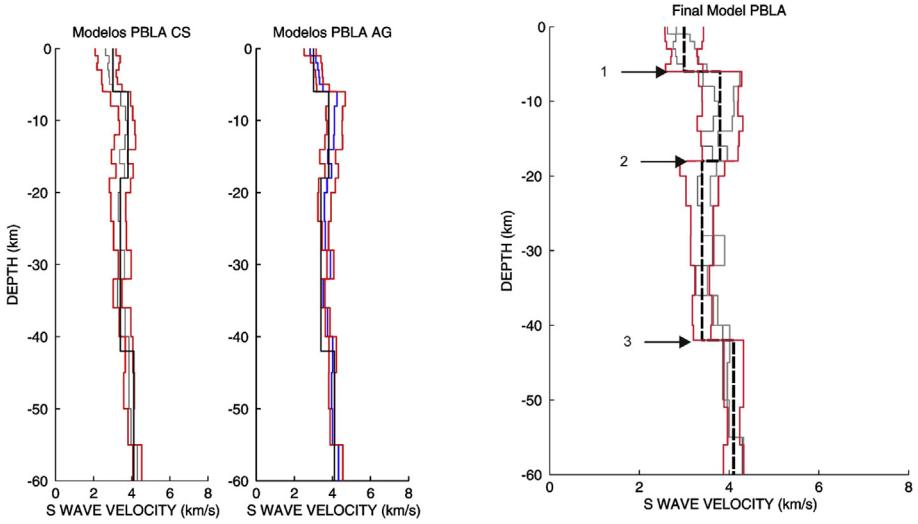

Fig. 14. The far left plot shows the average model beneath PBLA station using SA and its respective standard deviation. The central plot shows the average model beneath PBLA station using GA and its respective standard deviation. The far right plot shows the final model in dashed line for WC obtained at PBLA station with the inversion of 48,000 models using GA and 40,000 models using SA. Four layers are shown in the final model and the Moho is placed at 43 km. Gray lines show the average of both SA and GA plus and minus a standard deviation.

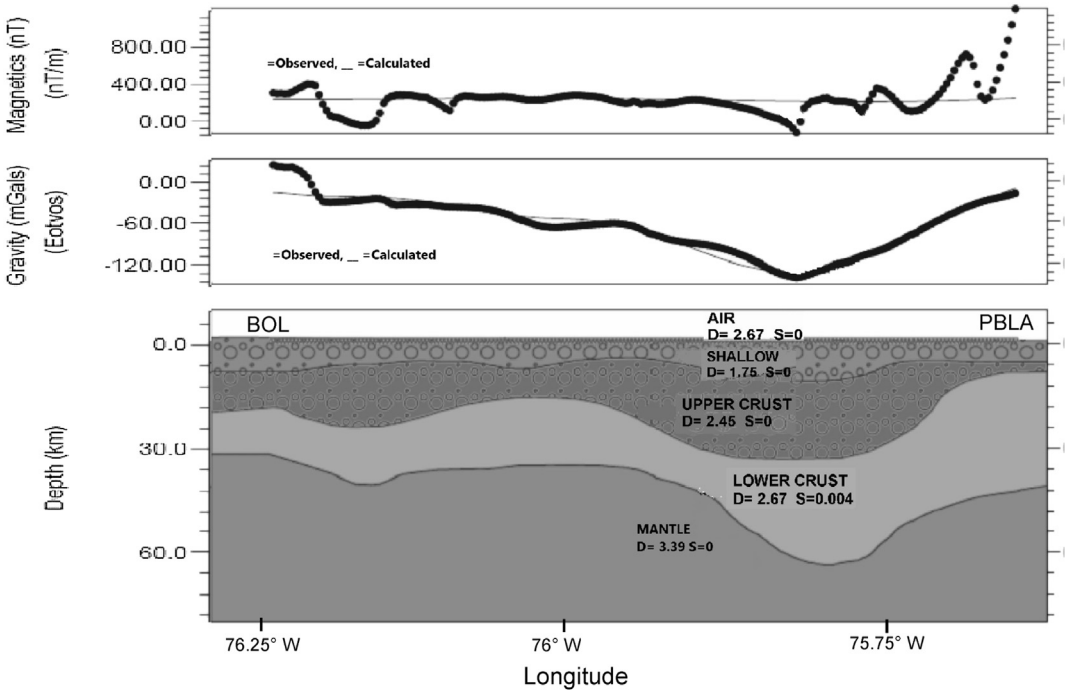

Fig. 15. Model profile from inversion. The gravity and magnetic response are shown for different layers. (Taken from Alexander et al., 2010).

shows, in general terms, that the proposed model constrains well the observed velocity variation.

On the other hand, the WC is composed of metamorphic rocks, toleitic basalts, mafic andesites, quartz diorites; the most common rock types are sandstones, greywackes, lutites and mafic rocks (green rocks). There are two types of rocks: the rocks from igneous origin with mafic and ultramafic composition; and the rocks from sedimentary origin from deep oceanic basins. The predominant rocks are among the igneous rocks, the basaltic rocks and related kinds. The results show that in the layer at depths between 2 and 20 km the wave velocity is 0.17 km s^{-1} greater than the maximum obtained in the Table 12. In general terms, the proposed model also represents well the observed velocity variation.

6. Conclusions

- This paper presents a pioneering study about the crustal velocity structure beneath two stations at the Western Cordillera (WC) and Central Cordillera (CC) in Colombia using receiver functions along with a genetic algorithm (GA) and a Simulated Annealing Algorithm (SA) in order to constrain better solutions of the velocity structure model.
- The Andean crustal structure was estimated beneath the seismic station BOL for the WC, and beneath the seismic station PBLA for the CC through the inversion of receiver functions that were compared by semblance of the stacked functions for both observed and synthetic ones. The results of the models for average velocity are presented by relations of depth versus shear wave velocity.
- In station BOL, the models for Sandwich group and Alaska group have differences due to the lateral variation of the structure. The Conrad and Moho discontinuities are located at 20 and 40 km deep respectively.
- In station PBLA, the models for Ridge group and Aleutian group have differences also due to lateral variations of the structure. The Moho discontinuity is located at 43 km deep.
- The azimuthal dependence of the receiver functions suggests that there are lateral variations of the structure. However, the approximation of the final average profile obtained beneath each station corresponds to simple models of velocity structure.
- A moderate low velocity zone was found between 20 and 40 km depth beneath station BOL at the WC.
- The observations of the crustal structure using database from the Alps, the Tibet, and the Andes show acceptable coherence in the values of P-wave velocity.

Table 12
P-wave velocity for different depths obtained for the Alps, Tibet, and Andes crustal structure (adapted from Christensen and Mooney, 1995).

Depth (km.)	Average Vp (km/s)	Standard deviation	Vp (km/s) range
0–5	5.69	±0.67	$5.02 < Vp < 6.72$
5–20	6.38	±0.43	$6.04 < Vp < 6.2$
20–30	6.65	±0.43	$6.25 < Vp < 7.08$
30–35	6.81	±0.40	$6.41 < Vp < 7.31$
35–45	6.96	±0.43	$6.53 < Vp < 7.39$

Acknowledgments

The authors want to express their gratitude to COLCIENCIAS, for its funding through the project 1113-333-18668; also to Universidad del Quindío for the sponsorship through the Project No 333 coordinated by the Vice-Chancellor Office for Research, and to Universidad Nacional at Bogota for the funding of the geophysical surveying campaign in the study zone. Special thanks are also expressed to Seismological Observatory at Universidad del Quindío (OSQ) for the installation of the broadband seismic stations used in this work and for its support with instrumentation and maintenance of the seismic stations BOL and PBLA. Finally, the authors also want to thank P. Wessel and W. Smith, for providing the software GMT (Graphics Mapping Tools) for the activities of map processing.

References

Alexander, G.C., Hernandez, O., Montes, L., Monsalve, H., Vargas, C.A., 2010. Modelamiento de la Corteza terrestre en un sector de los Andes Colombianos a partir de datos de campos potencias satelitales, aerotransportados y terrestres. Earth Sci. J.. Submitted.

Ammon, C.J., Randall, G.E., Zandt, G., 1990. On the nonuniqueness of receiver function inversions. J. Geophys. Res. 95 (10), 303–315.

Ammon, C.J., 1991. The isolation of receiver effects from teleseismic P waveforms. Bull. Seism. Soc. Am. 81, 2504–2510.

Ammon, C.J., Zandt, G., 1993. The receiver structure beneath the southern Mojave Block. Bull. Seism. Soc. Am. 83, 737–755.

Baker, G.E., Minster, J.B., Zandt, G., Gurrolla, H., 1990. Constraints on crustal structure and complex Moho topograhy beneath Piñon Flat, california, from teleseismic receiver functions. Bull. Seismol. Soc. Am. 86, 1830–1844.

Botero, G., 1963. Contribución al conocimiento de la geología de la zona central de Antioquia. Anales Fac. Minas 57, 1–107. Medellín.

Bump, H.A., Sheenan, A.F., 1998. Crustal thickness variations across the northern Tien Shan fron teleseismic receiver functions. Geophys. Res. Lett. 25, 1055–1058.

Burdick, L.J., Langston, C.A., 1977. Modeling crustal structure through the use of converted phases in teleseismic body waveforms. Bull. Seismol. Soc. Am. 67, 677–692.

Christensen, N.I., Mooney, W.D., 1995. Seismic velocity structure and composition of the continental crust: a global view. J. Geophys. Res. 100, 9761–9788.

Cruz, A., 2000. Inversión Global con Algoritmos Genéticos y Cristalización Simulada, Aplicada a Función Receptor: Modelos Estructurales de Velocidades para la Corteza en la República de México, pp. 124–136. Ciudad de Mexico.

Feininger, T., Barrero, D., Castro, N., 1972. Geología de parte de los departamentos de Antioquia y Caldas (Subzona II-B). Ingeominas. Bol. Geol. 20 (2), 1–173. Bogotá.

Florez, J.A., Osorio, L.M., 2010. Determinación de modelo Unidimensional de velocidad en el centro occidente Colombiano utilizando tomografía sísmica local. In: Proyecto de grado, Facultad de Ingeniería, programa de ingeniería Civil. Universidad del Quindío, p. 80.

Grosse, E., 1926. Estudio geológico del terciario carbonífero de Antioquia en la parte occidental de la cordillera central de Colombia. Verlag Von Dietrich Reimer (Ernst Vohsen), Berlín, p. 361.

Gurrola, H., Baker, G.E., Minster, J.B., 1995. Simultaneous time-domain deconvolution to the computation of receiver functions. Geophys. J. Int. 120, 537–543.

Herrmann, R.B., Ammon, C.J., 2002. Computer Programs in Seismology, Version 3.20. report. Saint Louis University.

Jaramillo, J., 2010. Sismicidad en la zona norte del Valle y Quindío con registros de las estaciones de banda ancha Bolivar y Peñas Blancas: Periodo 2007 – 2009. In: Proyecto de grado, Facultad de ingeniería-Programa de ingeniería Civil. Universidad del Quindío. En edición.

Kellogg, J.N., Vega, V., 1995. Tectonic development of Panama, Costa Rica and the Colombian Andes: constraint from global positioning system geodetic and gravity. Geol. Am. Bull., 75–90 special paper, 295.

Kroonemberg, S., 1982. A grenvillian granulite belt in the Colombian Andes and its relations to the Guiana shield. Geol. Mijnbouw 61, 325–333.

Laarhoven, V., Aarts, E.H.L., 1989. Simulated Annealing: an introduction. Stat. Neerlandica 43, 31–52.

Langston, C.A., 1977. Corvallis, Oregon, crustal and upper mantle structure from teleseismic P and S waves. Bull. Seismol. Soc. Am. 67, 713–724.

Langston, C.A., 1979. Structure under Mount Rainier, Washington, inferred from teleseismic body waves. J. Geophys. Res. 84, 4749–4762.

Lapp, D.B., Crosson, R.S., Owens, T.J., 1990. P-waveform analysis for local subduction geometry south of pudget Sound, Washington. Pure App. Geophys. 133, 349–355.

Mangino, S.G., Zandt, G., Ammon, C.J., 1993. The receiver structure beneath Mina, Nevada. Bull. Seism. Soc. Am. 83, 542–560.

Metropolis, N., Rosenbluth, A.W., Rosenbluth, M.N., Teller, A.H., Teller, E., 1953. Equation of state calculations by fast computing machines. J. Chem. Phys. 21 (6), 1087. http://dx.doi.org/10.1063/1.1699114.

Morales, Y.A., 2010. Implementación de un algoritmo genético y uno de cristalización simulada para la generación de modelos corticales de estructura y velocidad usando función receptor. In: Proyecto de grado, Facultad de Ingeniería, programa de ingeniería electrónica. Universidad del Quindío (in press).

Nivia, A., 1994. The Bolivar mafic-ultramafic complex, SW Colombia: the base of an obducted oceanic plateau. J. South Am. Earth Sci. 999, 1–10.

Ozalaybey, S.M., Savage, M.K., Sheenan, A.F., Louie, J.N., Brune, J.N., 1997. Shear wave velocity structure in the Northern Basin and range province from the combined analysis of receiver function and surface waves. Bull. Seismol. Soc. Am. 87, 183–199.

Owens, T.J., Zandt, G., Taylor, S.R., 1984. Seismic evidence for an ancient rift beneath the Cumberland Plateau, Tennessee; a detailed analysis of broadband teleseismic P waveforms. J. Geophys. Res. 89, 7783–7795.

Owens, T.J., 1987. Crustal structure of the Adirondacks determined from broadband teleseismic waveform modeling. J. Geophys. Res. 92, 6391–6401.

Restrepo-Pace, P.A., 1995. Late Precambrian to Early Mezsozoic Tectonic Evolution of the Colombian Andes, Based on Geochronological, Geochemical and Isotopic Data. PhD thesis. University of Arizona, Tucson, p. 194.

Shibutani, T., Sambridge, M., Kennett, B., 1996. Genetic algorithm inversion for receiver functions with application to crust and uppermost mantle structure beneath. East. Australia. Geophys. Res. Lett. 23, 1829–1832.

Silver, P.G., 1996. Seismic anisotropy beneath the continents probing the depths og geology. Ann. Rev. Earth Planet. Sci. 24, 385–432. http://dx.doi.org/10.1146/annurev, earth.24.1.385.

Zhang, J., Langston, C.A., 1995. Dipping structure under Dourbes, Belgium, determined by receiver function modeling and inversion. Bull. Seismol. Soc. Am. 85, 254–268.